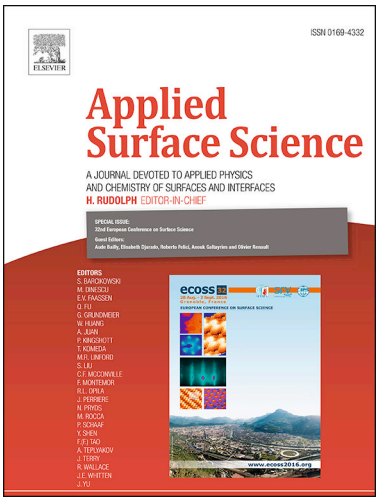

Full Length Article

Micro-cracks on crosslinked Poly(dimethylsiloxane) (PDMS) surface treated by nanosecond laser irradiation

Yu Deng, Wensheng Hong, Junfeng He, Zhongning Guo, Ying Chen, Zhigang Huang

PII: S0169-4332(18)30867-5
DOI: https://doi.org/10.1016/j.apsusc.2018.03.181
Reference: APSUSC 38929

To appear in: *Applied Surface Science*

Received Date: 2 January 2018
Revised Date: 22 March 2018
Accepted Date: 22 March 2018

Please cite this article as: Y. Deng, W. Hong, J. He, Z. Guo, Y. Chen, Z. Huang, Micro-cracks on crosslinked Poly(dimethylsiloxane) (PDMS) surface treated by nanosecond laser irradiation, *Applied Surface Science* (2018), doi: https://doi.org/10.1016/j.apsusc.2018.03.181

Micro-cracks on crosslinked Poly(dimethylsiloxane) (PDMS) surface treated by nanosecond laser irradiation

Yu Deng[a,b,c], Wensheng Hong[b], Junfeng He[a], Zhongning Guo[a,b], Ying Chen[c], Zhigang, Huang[a,*]

[a]School of Electromechanical Engineering, Guangdong University of Technology, Guangzhou, China

[b]Guangzhou Key Laboratory of Nontraditional Machining and Equipment, Guangdong University of Technology, Guangzhou, China

[c]Guangdong Provincial Key Laboratory of Functional Soft Condensed Matter, Guangdong University of Technology, Guangzhou, China

* response author
Zhigang Huang
Email: huangzg@gdut.edu.cn
Address: Waihuan Xi Road 100
Higher Education Mega Center
Guangzhou 51006, China
Tel: +86-20-39322412

Micro-cracks on crosslinked Poly(dimethylsiloxane) (PDMS) surface treated by nanosecond laser irradiation

Yu Deng[a,b,c], Wensheng Hong[b], Junfeng He[a], Zhongning Guo[a,b], Ying Chen[c], Zhigang, Huang[a,*]

[a]School of Electromechanical Engineering, Guangdong University of Technology, Guangzhou, China

[b]Guangzhou Key Laboratory of Nontraditional Machining and Equipment, Guangdong University of Technology, Guangzhou, China

[c]Guangdong Provincial Key Laboratory of Functional Soft Condensed Matter, Guangdong University of Technology, Guangzhou, China

Abstract: Surface morphology plays a critical role in the functionality of PDMS. In this work, micro-cracks were prepared on PDMS surfaces by nanosecond pulsed laser irradiation under ambient conditions. To fully investigate the resulting morphologies and the underlying processing mechanism, confocal microscopy, scanning electron microscopy (SEM), μ-Raman, 2D Raman and atomic force microscope (AFM) methods were employed to observe the laser treated PDMS samples. The results reveal that the micro cracks are the dominated morphology along the laser scanning routes, with lengths ranging from 56μm to 113μm while the angles varied from 40° to 90°. To control crack propagation, the effect of laser fluence and scanning speed on the topography of the cracks was studied and a thermal-stress model was established to explain the propagation process. It is concluded that laser irradiation is an easy method of pattern PDMS surface with micro/nano dual scale structures.

Keywords: micro-cracks, nanosecond laser irradiation, surface morphology, laser ablation, crack propagation

1. Introduction

PDMS is a special polymer characterized by high optical transparency, biocompatibility, gas permeability, mechanical flexibility, stability and mobility[1]. As a result, it is widely used in

Abbreviation
1. Poly(dimethylsiloxane) (PDMS)
2. scanning electron microscope (SEM)
3. atomic force microscope (AFM)
4. micro-electro-mechanic systems (MEMS)

optical waveguides, medical devices, gas sensors, micro-electrical-mechanical systems (MEMS) and microfluidic chips[2,4]. Micro patterns, like pillars, holes, wells, wrinkles, cracks, and even nanostructures, can be fabricated on its surface to improve its performance in regard to cell alignment, cell adhesion and wettability[4-6]. Because of such remarkable improvements, it has been used in bio-actuators, cell differential control, cell sorting and droplet manipulation[7-10].

Clean room technologies, especially photolithography and hot-embossing, are the most common methods of preparing a PDMS surface[11-14]. However, these methods require an ultraclean working environment, and the whole process becomes highly complex[12]. In addition, the molds used to form the patterns on the surface are difficult to fabricate[11]. 3D printing, on the other hand, can easily produce complex surface morphologies on PDMS[15], but such processes are relatively slow[16]. It is still a challenge to functionalize a PDMS surface in a economical and time-saving manner.

Because of its simplicity and high efficiency, the use of laser machining for PDMS surface patterning has attracted great attention from researchers. Nanosecond, picosecond and femtosecond lasers have all been employed to alter PDMS surfaces without affecting the bulk PDMS, because they affect only small volumes[17,18]. Among these, nanosecond laser machining is the most promising method due to its ability to produce acceptable quality at a relatively low cost. Photochemical and photo-thermal mechanisms have been proposed to explain the laser-induced material removal process, with the goal of predicating the final machining quality[19,20]. Experimental research has been carried out to investigate the impact of the process parameters, in terms of laser fluency, wavelength, overlap, scanning speed and working environment on the machining precision and process efficiency[19,21,22]. However, few researchers have specifically addressed the possibility of micro-crack formation on a PDMS surface by a nanosecond laser.

In this paper, we investigate the generation of micro-cracks on PDMS surfaces via nanosecond laser treatment. A series of experiments revealed that the lengths and orientations of the micro-cracks could be controlled. Based on the experimental results and changes in the Young's modulus and chemical composition of the surface, a thermal-stress model is proposed for crack propagation. Given its advantages of cost-effectiveness and simplicity,

nanosecond laser irradiation may be a promising method of micro-crack-pattern formation for future applications.

2. Materials and method

2.1 PDMS

The PDMS (Sylgard 184, Dowcorning) was purchased from Huawen Technics Co, and the base and the curing agent were mixed in a weight ratio of 10:1. The mixture （a total of 2 g） was poured into a cell culture plate with a diameter of 35mm, and then cured at 80°C for an hour. The resulting PDMS samples were about 3mm in thickness. Before the nanosecond laser treatment, the cured PDMS sample was first cleaned with ethanol and then with DI water for 10 min. The same cleaning process was employed after laser irradiation. After cleaning, the samples were dried overnight inair ambient.

2.2 Nanosecond laser treatment

PDMS-elastomer samples were treated using a Q-switch ultraviolet laser (SLCu-5030i, Strong Laser) with a wavelength of 355nm. Fig. 1 (a) shows the schematic of the process. A10ns laser pulse with a repetition rate of 30 KHz was reflected from several mirrors and finally focused on the PDMS surface by a lens with a focal distance of 22mm. The laser was focused on a spot with diameter of 20 μm. The laser power was tuned at range of 2.1 W-3.4 W by a computer controlled attenuator. The CCD provided an opportunity to observe the process online. The X-Y-Z stage on which the PDMS sample was mounted was driven by three service-motors to provide the scanning route, as indicated in Fig. 1 (b).

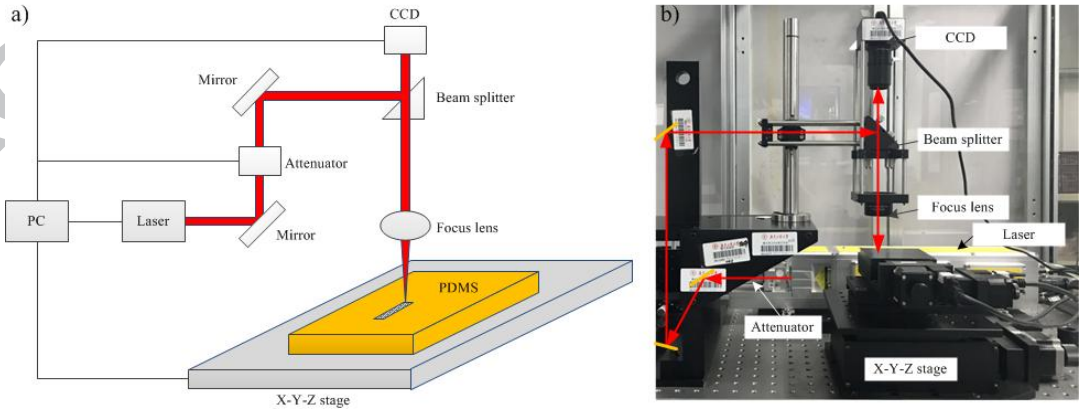

Fig. 1 The Schematic of Nanosecond laser ablation and the machine, the red arrow indicating the laser path and the yellow line indicating the mirrors that are not shown in the figure

Laser fluence and scanning speed are the main factors that determine the morphology of the

treated surface. Thus we conducted series of experiments using the conditions listed in Table 1. The laser fluence levels used in the experiments were set by the laser power levels of 2.3 W, 2.7 W and 3.1 W, respectively. For the sake of reproducibility, four samples were each treated three times.

Table 1 The experimental conditions

Parameters	**values**
Laser fluence (J / cm^2)	24.5, 28.5, 32.9
Scanning speed (mm/s)	300, 400, 500, 600, 700, 800, 900, 1000

2.3 Micro-cracks observation

The micro-cracks on the treated PDMS were characterized using a confocal microscope (OSL400, Olympus) and a SEM (SU8010, Hitachi). Since PDMS is an insulator, a 10nm-thick layer of platinum was coated on the surface before SEM imaging. The micro-crack length (l) and angle (θ) are illustrated in Fig. 2, and were obtained by analyzing the microscope images via ImageJ. Each value represents the mean value of five independent measurements made in various sample locations.

Further characterization of the surface was carried out by μ-Raman (LabRAM HR800, Horiba) and AFM (DimensionFastScan, Bruker) to confirm any modification of the chemical and mechanical properties. A Raman shift between 400 cm^{-1} and 3200 cm^{-1} with a resolution of 1 cm^{-1} was observed with a 532nm laser activation and 100x objective magnification. Four points that represent the four main areas of the machining zone were measured. In addition, two small planes, the treated surface (4μm×10μm) and the cross section (4μm×10μm), were scanned based on spectra between 513 cm^{-1} to 518cm^{-1} to check the distribution of the mono-crystalline silicon. A square (10μm×10μm) was scanned by AFM to determine Young's modulus (E) with a tip (ScanAsyst-Air) in an absolute model of QNM developed by Bruker. Each E value was automatically determined using NanoScope Analysis 1.5 and corresponded to the average of 9 squares measured in the near, the middle and the distant fields (3 of each), as defined in Fig. 2.

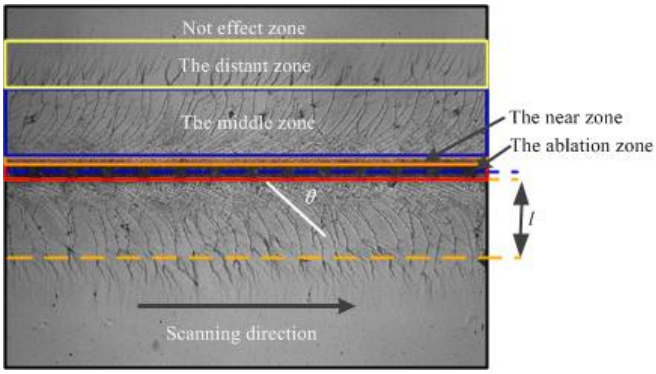

Fig. 2 The definition of different parts of the sample and the properties of the micro-cracks

3. Results

3.1 The crack morphologies

The morphology of PDMS is critical to its functionality. Fig. 3 presents a typical morphology of a treated surface processed with a laser fluence of 28.5J/cm^2 and a scanning speed of 500mm/s. Fig. 3 (a), (b) and (c) are the start, the middle and the end parts of the laser scanning route, respectively. The near zone, which is the closet zone to the scanning route, has a net-like morphology and grain sizes that range from hundreds of nm to several microns, as indicated in Fig. 3 (d) (this image has been rotated 90° counter-clock wise for better presentation). The middle zone shown in Fig. 3 (e) is dominated by an array of orientation micro-cracks with widths of about 400nm. Fig.3 (f) is the SEM image of the distant zone in which few cracks are observed and their width go down to about 100nm. It is worth noting that after several days, the cracks in the distant zone disappear because of the PMDS self-healing ability. The high-magnification image of the starting section shown in Fig. 3 (g) indicates that there are clearly separated three zones, same as the middle part (Fig. 3(h)). One interesting phenomena should be pointed out is that, ahead of the scanning route, micro-cracks propagated radically from a center defined by the start of the first laser pulse. On the other hand, the end part in Fig. 3 (i) has clear micro-cracks arrays at the radial direction, and the width of the near zone is much smaller (about 1μm)than the one in the middle part (about 10μm).

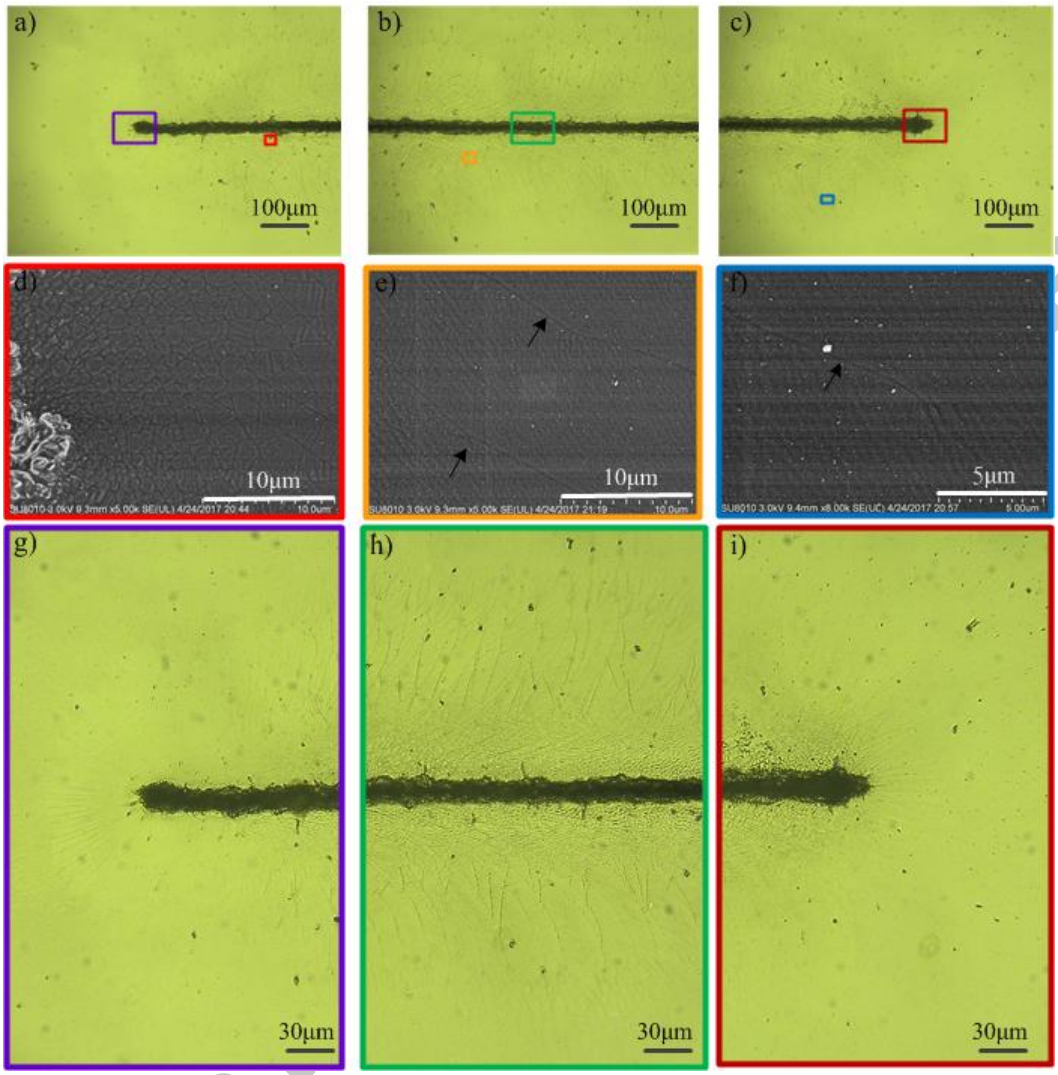

Fig. 3 Different parts of the treated PDMS surface with laser fluence of 28.5 J/cm^2 and scanning speed of 500mm/s. (a-c) show the start part, the middle part and the end part of the scanning route, respectively; (d-i) are the images at the locations marked in (a-c) by the rectangles in colors) and (d-f) are the SEM images at the near zone, middle zone and distant zone, while (g-i) are the zoom out images of the start part, the middle part and the end part of the scanning route, respectively

3.2 The impacts of process parameters

As is indicated above, the laser treatment was processed under a series of experimental conditions in order to fully study the effect of laser fluence and scanning speed on the crack regulation. Fig. 4 plots the influence of these parameters on the micro-crack angle and the length. As the scanning speed increases from 300 mm/s, the crack angle increases from slightly above 40° to 90° at any given laser fluence (Fig. 4 (a)). When the angle reaches 90°, further increase of the scanning speed causes the orientated crack to disappear rather than

increasing the angle. Even the processes performed at different laser fluences share similar trends, in that the rate of changes increases with the reduction on laser fluence. Regarding the length of the cracks presented in Fig. 4 (b), it decrease lineally along with the rise of the scanning speed. The minimum length is 56μm obtained at 800mm/s scanning speed and 24.5J/cm^2 laser fluence, and the maximum length is 113μm obtained at 300mm/s scanning speed and 32.9J/cm^2 laser fluence.

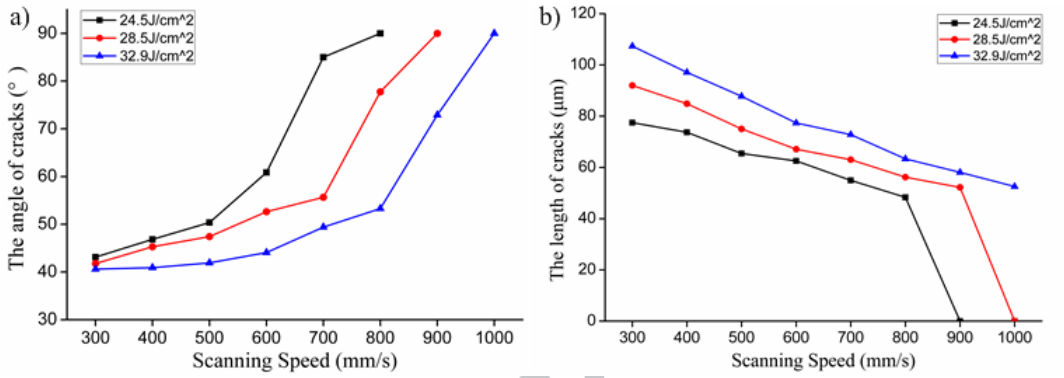

Fig. 4 The effect of laser fluence and scanning speed on micro-cracks

Fig. 5 shows the samples processed at scanning speed of 400mm/s and various laser fluences. At 32.9J/cm^2, as shown in Fig. 5 (a), the micro-cracks are about 110μm-long and 42° angles are formed along the scanning route. However, the PDMS is seriously burnt and sparkling particles are found in the near zone. In Fig. 5 (b), the micro-cracks are with 70μm long and 49° angles and corresponding to the sample treated at 28.5J/cm^2 but no sparkling particles were generated. The sample produced at 24.5J/cm^2 is presented in Fig. 5(c). The debris are found along the laser scanning route and some breaks in the line are also noted. Besides these, the absence of cracks along the route completely differs from the samples processed at higher laser fluence and the same scanning speed.

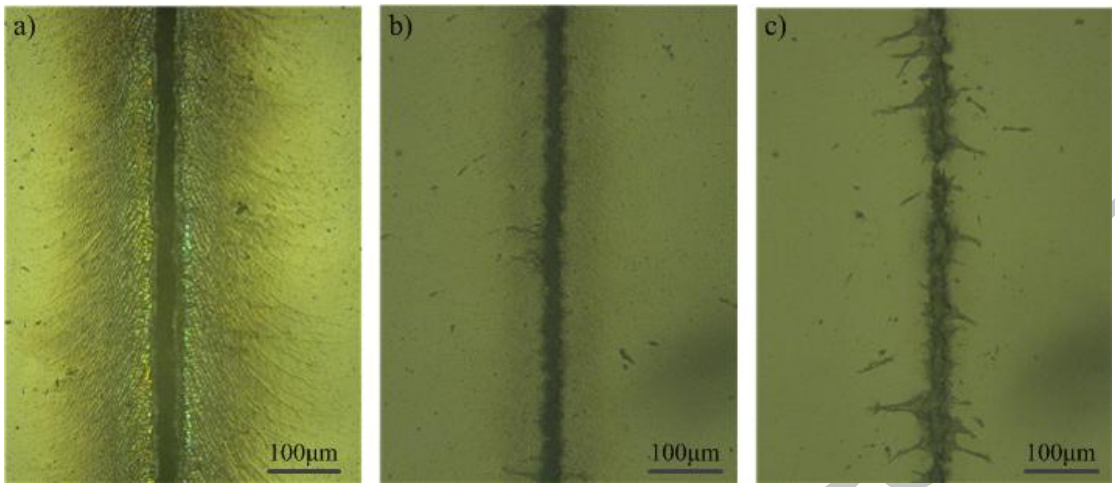

Fig. 5 Samples processed at scanning speed of 400mm/s and laser fluence of (a) 32.9J/cm^2, (b) 28.5/cm^2 and (c) 24.5J/cm^2

Fig. 6 shows the PDMS pieces processed at a laser fluence of 32.9J/cm^2 and various scanning speeds. As indicated in Fig. 6 (a), the sample treated at 400mm/s has a clean channel along the scanning route. Thus, the three typical zones described previously are present, and the related cracks are of length98μm and angle 46°. The sample processed at a scanning speed of 600mm/s is also shown in Fig. 6 (b). It is clear that cracks are generated along the route although there is no direct laser spot overlap at this speed. However, there are fewer cracks than in the sample generated at 400 mm/s. When the scanning speed increases to 1000mm/s, a few small cracks vertical to the scanning route are produced, but they disappeared after about two weeks self-healing.

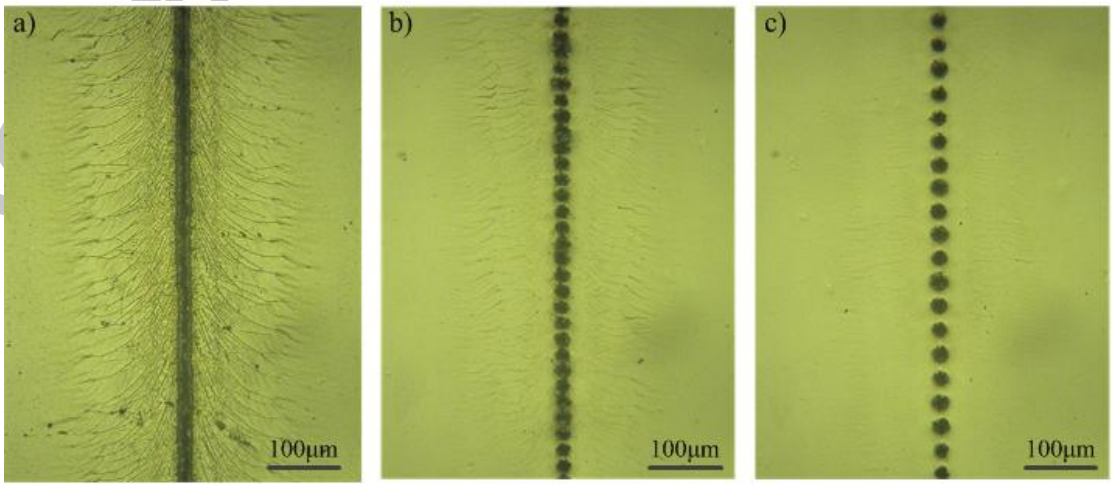

Fig. 6 Samples processed at laser fluence of 32.9J/cm^2 and scanning speed of (a) 400mm/s, (b) 600mm/s and (c) 1000mm/s

3.3 The AFM and μ-Raman

Fig. 7 presents the properties of the PDMS surface. Young's modulus of the sample treated with 28.5J/cm^2 laser fluence is dramatically increased as plotted in Fig. 7 (a). Young's modulus of the untreated PDMS is 2.1MPa, and the nanosecond laser treatment gives an increaseto more than 15MPa. When the laser scans at 800 mm/s, the value of Young's modulus is 16MPa on average. However, as the scanning motion slows, it goes up to 16.7MPa at 600mm/s and 22.9MPa at 400mm/s.

The Raman spectra of the sample treated with laser fluence of 28.5J/cm^2 and scanning speed of 400mm/s has been specifically studied. The typical peaks of PDMS in the Raman spectra are listed in Table 2 as well as the plot in Fig 7 (b) (the Y offset between neighboring lines is 7000a.u.). Few differences are observed between the distant and middle zones, which indicates that the laser treatment produces no chemical differences between them. However, significant differences are noted at the near zone and among the sparkling particles. Further, the intensity at the PDMS peaks experiences a large drop and a sharp peak appears in the Raman shift between 513-518cm^{-1}. This new peak is attributed to mono-crystalline silicon. To determine the distribution of the mono-crystalline silicon formed by the laser, 2D Raman was performed and the results are shown in Fig. 7 (c) and (d). Fig. 7 (c) is the distribution of the mono-crystalline silicon in the cross-section, indicated by the dash line. The mono-crystalline silicon is generated along the wall of the laser scanning route and its concentration peaks at the very edge of the surface. On the other hand, as indicated in Fig. 7 (d) (the distribution of mono-crystalline silicon on the surface, indicated by the rectangles), the mono-crystalline silicon is distributed through the surface but the concentration decreases on moving further away from the scanning route. It is interesting to note that a high concentration of mono-crystalline silicon is present in the sparkling particles.

Table 2 The typical peaks of PDMS and the corresponding chemical bonds[23]

Raman shift (cm^{-1})	**the corresponding chemical bonds**
488	Si-O-Si symmetric stretching
685	Si-CH_3 symmetric rocking
709	Si-C symmetric stretching
787	CH_3 asymmetric rocking

	Si-C asymmetric stretching
859	CH_3 symmetric rocking
1262	CH_3 symmetric bending
1411	CH_3 asymmetric bending
2909	CH_3 symmetric stretching
2970	CH_3 asymmetric stretching

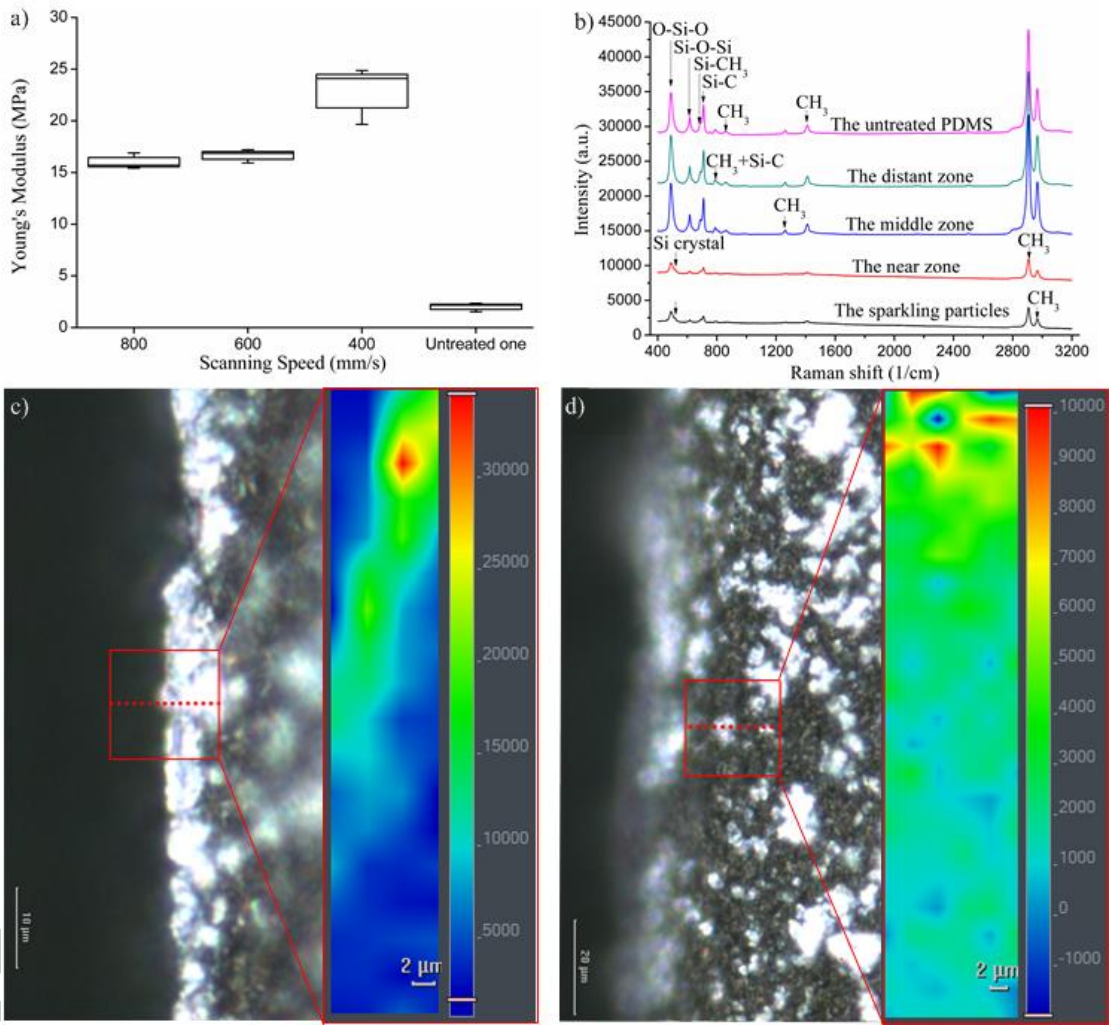

Fig. 7 The properties of the PDMS surface, (a) young's modulus, (b) μ-Raman, (c) 2D Raman of cross-section based on spectra between 513-518cm^{-1} and (d) 2D Raman of surface based on spectra between 513-518cm^{-1}

4. Discussion

4.1 Modification of the surface properties

As previous mentioned, the cross-linked PDMS is implemented in many fields for its excellent mechanical and chemical properties These properties result from its flexible

molecular backbone(Fig. 8). After laser irradiation, the PDMS experiences significant transformation in chemical composition during the laser irradiation process as indicated by Raman spectra. The intensities of the peaks indicating Si-O-Si, Si-C and CH_3 are reduced sharply. With laser induced photo-thermal effect, the Si-C bonds are firstly broken since these bonds are weaker (30 kcal/mol) than Si-O-Si. Consequently, CH_3 radicals and other polymer radicals are generated[24]. The CH_3 radical reacts with other radicals leading to the hydrogen abstraction and methane formation. The decrease in the peak of the Si-O-Si bonds means that these bonds are degraded, corresponding to the formation of mono-crystalline silicon. However, the G-bands and D-bands mentioned in ref. [25], which indicate the carbon generated from several tens of laser pulses acting on the same location, are not found in the Raman spectra of the treated sample. In fast laser scanning, the laser overlap in the experiments ranged from 0.5 to 0.1. Thus a maximum of 50% of the area overlaps between neighboring laser spots. Thus, any given location experiences two laser pulses at maximum, and this is far fewer than the number listed in ref. [25].

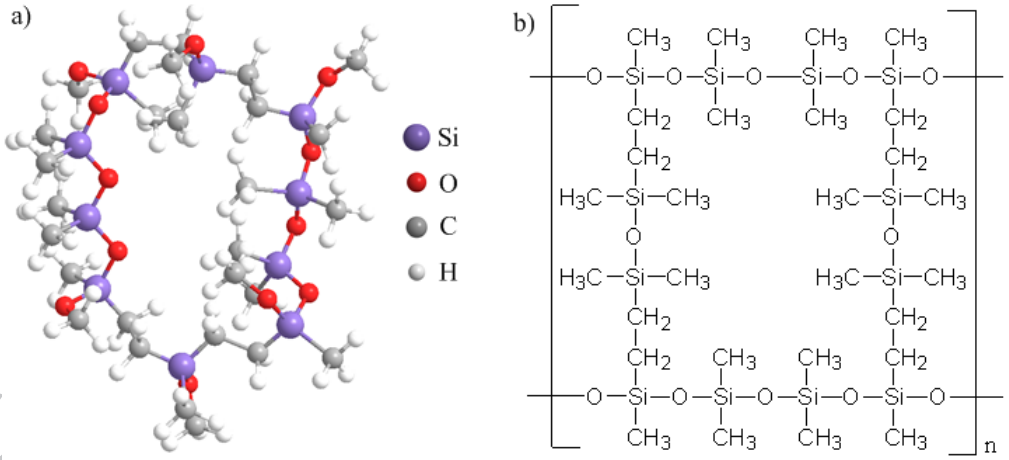

Fig. 8 The cross-linked PDMS， a) the 3D structure and b) the linear formula of cured PDMS

In addition to experiencing chemical transformations, the PDMS surface also changes greatly in its mechanical properties, particularly Young's modulus. This is mainly attributed to the laser-induced thermal effect. At low temperature (<200 ℃), Young's modulus slightly increases to about 8MPam then stays constant as the cross-linking process continues. This stems from the imprecision in the quantities of the PDMS base and the curing agent used[26]. However, in our study, the resulting Young's modulus of the laser treated PDMS is much higher than that. The primary factor contributing to it is that, with laser irradiation, the

temperature is much higher than 200℃, thus thermal decomposition and photochemical reaction are inevitable. The resulting silicon particles (Fig. 7 (c,d)) are distributed on the surface, thus the maximum Young's modulus of the treated surface increases by a factor of almost 10.

4.2 The mechanism of cracks orientation

Micro-cracks represent the dominant treated surface morphology. To understand the formation of this morphology, a thermal-stress model is established in Comsol. Laser-induced thermal effects dominate this analysis and micro-cracks propagate in the direction of the maximum rate of energy release [27,28]. The thermal-stress module is used directly, in which, the laser fluence is defined by a pulsed heat flux on the PDMS surface (X-Y plane, Z=0) and it moves at the scanning speed. The heat flux (q) attributed to Gaussian laser fluence changes along the depth direction (Z) according to the Beer-Lambert law[29],

$$q(x,y,z,t)=q(0,l,0,0)\exp(-\alpha z)\exp\left[-2\frac{(x^2+(y-l-vt)^2)}{R^2}\right]pulse(\tau,1/f) \quad (1)$$

where l=35μm is the Y-offset, α=4.8×10^{-4}cm^{-1} is the absorption coefficient of PDMS at 355nm, v indicates the scanning speed, R presents the radius of laser spot on the surface and $pulse(\tau, 1/f)$ is the square wave with amplitude of 1, an on time τ=10ns and frequency f=30KHz.

Thus the temperature field in PDMS can be defined as $T(x, y, z, t)$ and it is achieved with consideration of the heat diffusion,

$$\begin{cases} k(\frac{\partial^2 T}{\partial x^2}+\frac{\partial^2 T}{\partial y^2}+\frac{\partial^2 T}{\partial z^2})+Q=\rho C_p\frac{\partial T}{\partial t} \\ T(x,y,z,0)=295K \\ -k(\frac{\partial t}{\partial n})_w=h(t_w-t_f) \end{cases} \quad (2)$$

where k=0.27W/(m·K) is the thermal conductivity of PDMS, ρ=1030Kg/m^3 is the density of PDMS, C_p=1461J/(Kg·K) is the specific heat of PDMS and its value is, and Q is the amount of heat per unit volume resulting from the laser irradiation. The PDMS is processed at an initial temperature of 295K, and w, h indicate the convection surface and convection coefficient.

The temperature field is coupled to the mechanical stress model via a thermal-stress module

in Comsol5.2. The specimen in the model is defined with dimensions of 50μm×120μm×50μm. The simulation boundaries are mechanically fixed vertices $u_x=u_y=u_z=0$ on the bottom surface (Z=-50μm).

When the von Mises stress exceeds the failure stress $\sigma_f=(2E\gamma_f/\pi c)^{0.5}$, in which E is Young's modulus, γ_f is failure surface energy and c is the crack length, the cracks grow. The cracks extend toward the direction where the energy release rate is maximized and the tensile stress dominates [30]. Therefore, we plot the Von Mises stress along Y axis in Fig. 9 (a) and (b) to verify the effect of laser scanning speed (300mm/s and 900mm/s, respectively) on the crack orientation at a laser fluence of 24.5J/cm^2, noting that the time in Fig. 9 is the delay time from the first laser pulse. As shown in the plots, the stress increases to 0.37MPa because of the first laser pulse action. There is no clear difference between these two cases before the second laser pulse loading. The stress distributions significantly differ from each other under the second laser pulse load because of the difference in the laser scanning speed. Changing the scanning speed changes the distance between the first and the second pulse (d), according to the following equation,

$$d = v / f \tag{3}$$

thus, the distance between the first and second pulses is 9 μm when the laser scans at a speed of 300 mm/s. At 900 mm/s, the distance is 27 μm. Consequently, two peaks at 35μm and 55μm can be observed at 300mm/s and three peaks (25μm, 58μm, 75μm) at 900mm/s. Fig. 9 (c-h) and (i-n) are the time slips of the simulation at laser scanning speeds of 300mm/s and 900mm/s, respectively. The same phenomena appears after the second laser pulse. It is clear that the thermal stress is affected by the second pulse irradiation. The impact is more significant at slower scanning speed, and as a result, the crack tip deflection angle increases with the laser scanning speed[31].

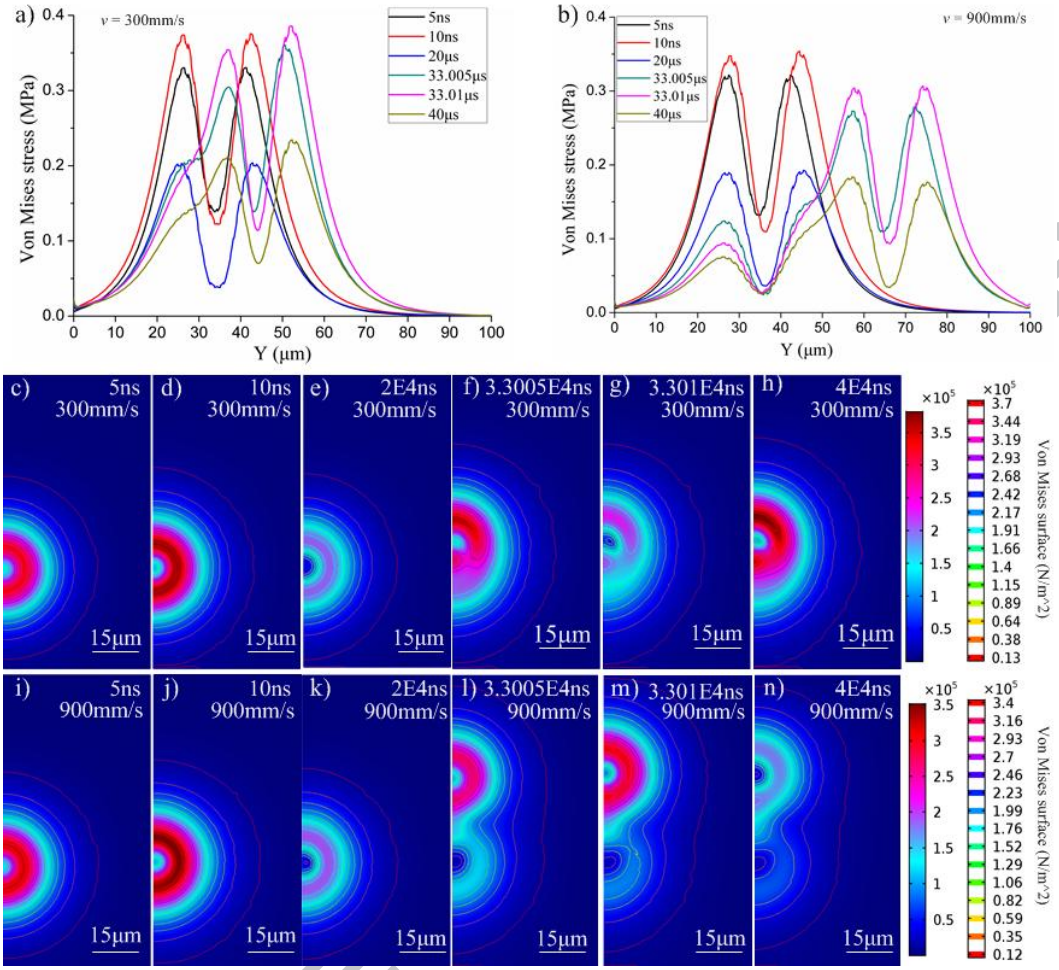

Fig. 9 The simulated Von Mises stress results, (a), (b) are Von Mises stress along Y axis at a laser fluence of 24.5J/cm^2 and laser scanning speed (300mm/s and 900mm/s, respectively), (c-h) are the time slips of the Von Mises stress distribution at a laser fluence of 24.5J/cm^2 and laser scanning speed 300mm/s, (c-h) are the time slips of the Von Mises stress distribution at a laser fluence of 24.5J/cm^2 and laser scanning speed 900mm/s.

Conclusions

A nanosecond laser-treated PDMS surface has been specifically studied by confocal microscopy, SEM, μ-Raman, 2D Raman and AFM, with the following conclusions: (i) mono-crystalline silicon is found on the treated surface by μ-Raman characterization and is distributed primarily along the edge of the channel and in the sparkling particles observed using 2D Raman, both of which are a result of the PDMS decomposition. (ii) Young's modulus dramatically increases to about 22.9MPa, around 10 times that of nature at PDMS, because of the further cross-linking process and the generation of mono-crystalline silicon. (iii) micro-cracks dominate the morphology of laser irradiated PDMS, and their length and

orientation are regulated by the laser pulse power and scanning speed. (iv) The numerical simulation and experimental results match closely. This confirms that the laser induced crack propagation is controlled by the laser-generated thermal-stress.

Our study specifically characterizes the properties of the PDMS irradiated by nanosecond laser. It is shown that nanosecond irradiation provides a promising way of patterning micro-cracks on PMDS due to its easy processing, and has great potential in industrial application of PDMS for its time-saving and cost-effectiveness.

Acknowledgements

The discussion on Raman analysis with Ruijie Xu and Guohui Huang of Guangdong University of Technology are greatly appreciated.

Funding: This work was supported by National Natural Science Foundation of China (grant number 51175091), China Postdoctoral Science Funding (grant number 2017M612610) , Foshan Municipal Science and Technology Bureau project (2015IT100162) and Project of young innovative talents in university of Guangdong (grant number 2015KQNCX027).

References

[1] L.Y. Ljungberg, Materials selection and design for structural polymers, Mater. Des. 24 (2003) 383.

[2] D. Cai, A. Neyer, R. Kuckuk, H. Heise, Raman, mid-infrared, near-infrared and ultraviolet–visible spectroscopy of PDMS silicone rubber for characterization of polymer optical waveguide materials, J. Mol. Struct. 976 (2010) 274-281.

[3] I.S. Hwang, Y.S. Kim, S.J Kim, B.K. Ju, J.H. Lee, A facile fabrication of semiconductor nanowires gas sensor using PDMS patterning and solution deposition, Sensor. Actuat. B: Chem. 136 (2009) 224-229.

[4] J. Heikenfeld, A. Jajack, J. Rogers, P. Gutruf, L. Tian, T. Pan, R. Li, M. Khine, J. Kim, J. Wang, Wearable sensors: modalities, challenges, and prospects. Lab Chip (2018) (DOI: 10.1039/c7lc00914c)

[5] B. Farshchian, J.R. Gatabi, S.M. Bernick, Park, S., G.H. Lee, R. Droopad, N. Kim, Laser-induced superhydrophobic grid patterns on PDMS for droplet arrays formation, Appl. Surf. Sci. 396 (2017) 359-365.

[6] K. Sun, H. Yang, W. Xue, A. He, D. Zhu, W. Liu, K. Adeyemi, Y. Cao, Anti-biofouling

superhydrophobic surface fabricated by picosecond laser texturing of stainless steel, Appl. Surf. Sci. 2018;436:263-267

[7] Y. Tanaka, K. Morishima, T. Shimizu, A. Kikuchi, M. Yamato, T. Okano, T. Kitamori, Demonstration of a PDMS-based bio-microactuator using cultured cardiomyocytes to drive polymer micropillars, Lab Chip 6 (2) (2006) 230-235.

[8] S.F. Toosi, S. Moradi, S.G. Hatzikiriakos, Fabrication of Micro/Nano Patterns on Polymeric Substrates Using Laser Ablation Methods to Control Wettability Behaviour: A Critical Review, Rev. Adhesion Adhesives 5 (1) (2017) 55-78.

[9] W. Ding, Y. Yang, Y. Zhao, S. Jiang, Y. Cao, C. Lu, Well-defined orthogonal surface wrinkles directed by the wrinkled boundary, Soft Matter 9 (14) (2013) 3720-3726.

[10] Y. Zhang, S. Park, K. Liu, J. Tsuan, S. Yang, T.H. Wang, A surface topography assisted droplet manipulation platform for biomarker detection and pathogen identification, Lab Chip 11 (3) (2011) 398-406.

[11] A.T. Abdulhussein, G.K. Kannarpady, A.B. Wright, A. Ghosh, A.S. Biris, Current trend in fabrication of complex morphologically tunable superhydrophobic nano scale surfaces, Appl. Surf. Sci. 384 (2016) 311-332.

[12] Y. Liu, P. Zhang, Y. Deng, P. Hao, J. Fan, M. Chi, Y. Wu, Polymeric microlens array fabricated with PDMS mold-based hot embossing, J. Micromech. Microeng. 24 (9) (2014) 095028.

[13] N.K. Tran, Y.C. Lam, C.Y. Yue, M.J. Tan, Manufacturing of an aluminum alloy mold for micro-hot embossing of polymeric micro-devices, J. Micromech. Microeng. 20 (5) (2010) 055020.

[14] E. Angeli, C. Manneschi, L. Repetto, G. Firpo, U. Valbusa, DNA manipulation with elastomeric nanostructures fabricated by soft-moulding of a FIB-patterned stamp, Lab Chip 11 (15) (2011) 2625-2629.

[15] N. Bhattacharjee, A. Urrios, S. Kang, A. Folch, The upcoming 3D-printing revolution in microfluidics, Lab Chip 16 (10) (2016) 1720-1742.

[16] H.N. Chan, Y. Chen, Y. Shu, Y. Chen, Q. Tian, H. Wu, Direct, one-step molding of 3D-printed structures for convenient fabrication of truly 3D PDMS microfluidic chips，Microfluid. Nanofluid. 19 (1) (2015) 9-18.

[17] P.A. Atanasov, N.E. Stankova, N.N. Nedyalkov, N. Fukata, D. Hirsch, B. Rauschenbach, S. Amoruso, X. Wang, K.N. Kolev, E.I. Valova, J.S. Georgieva, Fs-laser processing of medical grade polydimethylsiloxane (PDMS), Appl. Surf. Sci. 374 (2016) 229-234.

[18] A. Cunha, A.M. Elie, L. Plawinski, A.P. Serro, A.M.B. do Rego, A. Almeida, M.C. Urdaci, M.C. Durrieu, R. Vilar, Femtosecond laser surface texturing of titanium as a method to reduce the adhesion of Staphylococcus aureus and biofilm formation, Appl. Surf. Sci. 360 (2016) 485-493.

[19] A.D. Zweig, V. Venugopalan, T.F. Deutsch, stress generated in polymeric materials, J. Appl. Phys. 74 (6) (1993) 4181-4189.

[20] T. Lippert, laser application of polymers, in: T.K. Lippert (Eds.), Polymers and Light, Springer, Berlin Heidelberg, 2004, pp. 51-246.

[21] E. Bulushev, V. Bessmeltsev, A. Dostovalov, N. Goloshevsky, A. Wolf, High-speed and crack-free direct-writing of microchannels on glass by an IR femtosecond laser, Opt. Laser Eng. 79 (2016) 39-47.

[22] W. Wang, Y.Q. Liu, Y. Liu, B. Han, H. Wang, D.D. Han, J.N. Wang, Y.L. Zhang, H.B. Sun, Direct Laser Writing of Superhydrophobic PDMS Elastomers for Controllable Manipulation via Marangoni Effect, Adv. Funct. Mater. 27 (44) (2017) (DOI: 10.1002/adfm.201702946)

[23] S.C. Bae, H. Lee, Z. Lin, S. Granik, Chemical imaging in a surface forces apparatus: confocal Raman spectroscopy of confined poly(dimethylsiloxane), Langmuir 21 (13) (2005) 5685-5688

[24] K. Chenoweth, S. Cheung, A.C.T. van Duin, W.A. Goddard, E.M. Kober, Simulations on the Thermal Decomposition of a Poly(dimethylsiloxane) Polymer Using the ReaxFF Reactive Force Field, J. Am. Chem. Soc. 127 (2005) 7192-7202.

[25] N.E. Stankova, P.A. Atanasov, N.N. Nedyalkov, T.R. Stoyanchov, K.N. Kolev, E.I. Valova, J.S. Georgieva, A. St A, S. Amoruso, X. Wang, R. Bruzzese, fs-and ns-laser processing of polydimethylsiloxane (PDMS) elastomer: Comparative study, Appl. Surf. Sci. 336 (2015) 321-328.

[26] I.D. Johnston, D.K. McCluskey, C.K.L. Tan, M.C. Tracey, Mechanical characterization of bulk Sylgard 184 for microfluidics and microengineering, J. Micromech. Microeng. 24

(3) (2014) 035017.

[27] M. Chowdhury, X. Sheng, F. Ziebert, A.C.M. Yang, A. Sepe, U. Steiner, G. Reiter, Intrinsic stresses in thin glassy polymer films revealed by crack formation. Macromolecules 49 (23) (2016) 9060-9067.

[28] C. Zhao, H. Zhang, L. Yang, Y. Wang, Y. Ding, Dual laser beam revising the separation path technology of laser induced thermal-crack propagation for asymmetric linear cutting glass, Int. J. Mach. Tool Manu. 106 (2016) 43-55.

[29] D.F. Swinehart, The beer-lambert law, J. Chem. Educ. 39 (7) (1962) 333.

[30] C. Zhao, H. Zhang, Y. Wang, Semiconductor laser asymmetry cutting glass with laser induced thermal-crack propagation, Opt. Laser. Eng. 63 (2014) 43-52

[31] Y. Miyashita, M. Mogi, Study on a controlling method for crack nucleation and propagation behavior in laser cutting of glass. J. Solid Mech. Mater. Eng. 2 (12) (2008) 1555-1566.

Table 1 Experimental conditions

Parameters	**values**
Laser fluence (J / cm^2)	24.5, 28.5, 32.9
Scanning speed (mm/s)	300, 400, 500, 600, 700, 800, 900, 1000

Table 2 The typical peaks of PDMS and the corresponding chemical bonds[23]

Raman shift (cm^{-1})	**the corresponding chemical bonds**
488	Si-O-Si symmetric stretching
685	Si-CH_3 symmetric rocking
709	Si-C symmetric stretching
787	CH_3 asymmetric rocking
	Si-C asymmetric stretching
859	CH_3 symmetric rocking
1262	CH_3 symmetric bending
1411	CH_3 asymmetric bending
2909	CH_3 symmetric stretching
2970	CH_3 asymmetric stretching

Highlights

1. the micro-crack with length between 56-113μm and angle between 40°-90° is the main morphology on the surface of PDMS irradiated by nanosecond laser.
2. the propagation of the cracks is determined by thermal-stress and it is regulated by laser pulse power and laser scanning speed.
3. Raman spectra indicates that mono-crystalline silicon particles are generated by nanosecond laser and they mainly distribute along the scanning route.

Graphical abstract